Microscopic dynamics in simple liquids: a clue to understanding the basic thermodynamics of the liquid state

2004 J. Phys.: Condens. Matter 16 S309

(http://iopscience.iop.org/0953-8984/16/5/001)

INSTITUTE OF PHYSICS PUBLISHING JOURNAL OF PHYSICS: CONDENSED MATTER

J. Phys.: Condens. Matter **16** (2004) S309–S325 PII: S0953-8984(04)65478-6

Microscopic dynamics in simple liquids: a clue to understanding the basic thermodynamics of the liquid state

C Cabrillo[1], F J Bermejo[1,2], A Maira-Vidal[1], R Fernández-Perea[1], S M Bennington[3] and D Martin[3]

[1] Instituto de Estructura de la Materia, Consejo Superior de Investigaciones Científicas, Serrano 123, E-28006 Madrid, Spain
[2] Department of Electricity and Electronics, Faculty of Science, University of the Basque Country, PO Box 644, E-48080 Bilbao, Spain
[3] Rutherford Appleton Laboratory, Chilton, Didcot, Oxon OX11 0QX, UK

E-mail: embermejo@iem.csic.es

Received 30 June 2003, accepted for publication 2 July 2003
Published 23 January 2004
Online at stacks.iop.org/JPhysCM/16/S309 (DOI: 10.1088/0953-8984/16/5/001)

Abstract

The advent of inelastic x-ray scattering techniques has prompted a reawakened interest in the dynamics of simple liquids. Such studies are often carried out using simplified models to account for the stochastic dynamics that give rise to quasielastic scattering. The vibrational and diffusive dynamics of molten potassium are studied here by an experiment using neutron scattering and are shown to provide some clues to understand the basic thermodynamics of the liquid state. The findings reported here suggest ways in which the true complementarity of neutron and x-ray scattering may be profitably exploited.

(Some figures in this article are in colour only in the electronic version)

1. Introduction

The most characteristic feature of a normal (i.e. not deeply supercooled) liquid is the high mobility of its constituent particles. A polycrystalline solid may respond to an applied shear stress in a liquid-like fashion 'flowing' with [1] an effective viscosity

$$\eta \simeq s^2 k_B T / Dd \tag{1}$$

where s stands for the number of particles across a single crystallite, d the particle diameter and D for the self-diffusion coefficient. Surprisingly, equation (1) works well for liquid metals having viscosities about 10^{13} times smaller than that for the powders for which the recipe was proposed, provided that $s \approx 1$ [2]. The figure of merit here is thus the diffusion coefficient and early attempts were made on the grounds of kinetic theory to predict the value of such a quantity. The models used by such theories dealt with ensembles of hard spheres, where the

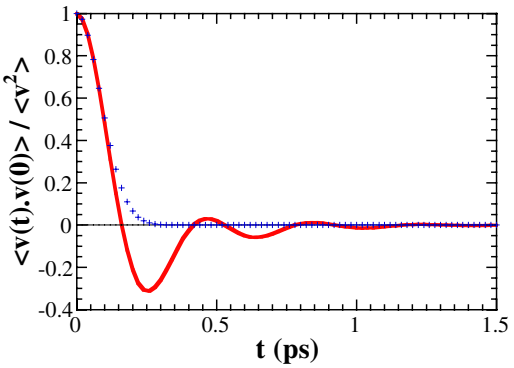

Figure 1. Velocity autocorrelation function for molten K at $T = 450$ K as evaluated by a molecular dynamics simulation carried out within the NVT ensemble for a system of 500 potassium atoms contained within a cubic box of length $L = 34.31$ Å and interacting through the potential described in [4]. The full line depicts the normalized velocity autocorrelation and crosses show the Gaussian approximation valid for short times.

basic parameters, apart from the diameter, are the temperature, the packing fraction and the pair distribution $g(r)$. The bare experimental facts have shown that such attempts, if applied to a simple liquid close to melting, overestimate D by a factor of about 1.5. The origin of such a discrepancy was found to be due to the highly entangled nature of particle motions within a dense liquid, as was illustrated by the seminal work of Rahman [3] on the velocity autocorrelation function $\langle v(t) \cdot v(0)\rangle$ of liquid Ar. For a liquid metal such as potassium, $\langle v(t) \cdot v(0)\rangle$ shows a noticeable oscillatory structure such as shown in figure 1. There we see how at rather short times ($t < 0.075$ ps), $\langle v(t) \cdot v(0)\rangle$ follows a Gaussian that is characteristic of a gas-like regime dominated by binary collisions and then a well defined oscillatory pattern appears. The origin of such a pattern is in part due to the oscillatory motions or 'cage' effect that a particle experiences for some characteristic time before relaxing towards local equilibrium. In molten K such motions persist up to ≈ 2 ps and are understood as well defined collective oscillations resembling the phonons of the crystal before melting. Their prominence in liquids such as molten alkali metals with respect to insulators such as Ar is also known to arise from details concerning the curvature of the interaction potential at its minimum [5].

The relevance of $\langle v(t) \cdot v(0)\rangle$ stems from the fact that its integral measures the self-diffusion coefficient and therefore the negative parts of the curve will yield a value for D significantly smaller than that calculated from the Gaussian representative of the gas regime. The presence within $\langle v(t) \cdot v(0)\rangle$ that is a *single-particle* quantity of an oscillatory structure reminds us of the complex nature of liquid dynamics at scales of a few picoseconds. Furthermore, it is precisely the wealth of details found at microscopic scales that provides us with a key to understanding the anomalies exhibited by some basic thermodynamic quantities of the liquid state. In fact, up to now the simplest thermodynamic function of a liquid, such as the specific heat, remains an elusive quantity to calculate with enough accuracy, and most of the tools able to predict the correct temperature dependence of $C_{\mathrm{p}}(T)$ once the crystal melts into its ordinary liquid range are of a phenomenological nature [6–8].

The bare experimental facts show that, contrary to what can be expected from what is known for crystals, i.e. $C_{\mathrm{v}}(T)$ increases with temperature up to the melting point where it approaches the Dulong–Petit value, the specific heat of a liquid metal usually decreases upon melting and continues decreasing as the temperature is raised [9]. Empirically [9], the specific

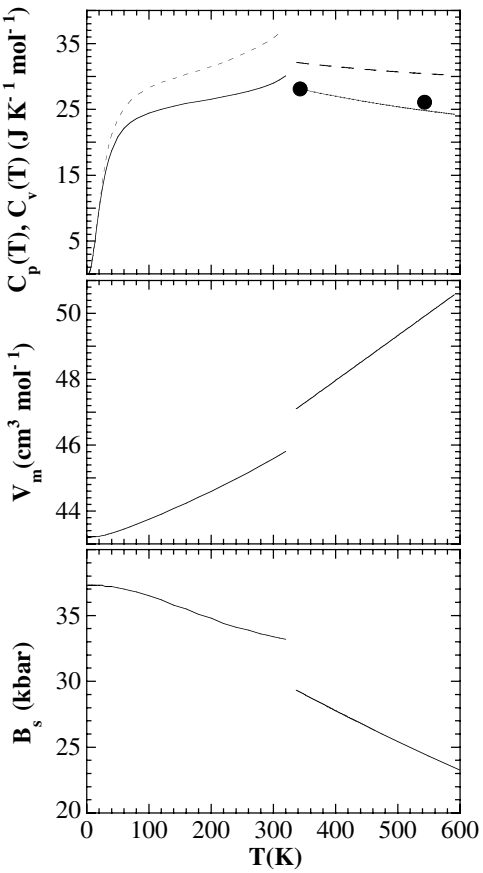

Figure 2. Thermodynamic data for crystalline and liquid potassium. The upper frame depicts the constant-volume (full) and constant-pressure (broken curves) specific heats of both solid and molten K. The middle frame shows the temperature variation of the mass density across the melting point. The lower frame shows the isotropic bulk modulus. Liquid data are taken from [9].

heat of liquid metals can be represented for a restricted range of temperature as

$$C_{\mathrm{p}}(T) = a + bT + cT^{-2} + dT^{2} \tag{2}$$

where a, b, c and d are constants, some of which may be zero or negative (i.e. liquid potassium data between melting $T_{\mathrm{m}} \approx 336$ and 1037 K are described by the following set of values: 37.179, -19.12×10^{-3}, 0 and 12.30×10^{-6}).

The negative values of a correction term to the Dulong–Petit value of $C(T)$ for a liquid was recognized as early as 1937 by Brillouin [10] who proposed that such a correction should vary from 0 at T_{m} to R at the critical point due to the progressive loss of shear waves as the temperature increases. An example of what has just been written is given by thermodynamic data for liquid potassium shown in figure 2 where it is shown that melting of the crystal is accompanied by a small change in volume (≈2.54%), a concomitant decrease in the isotropic bulk modulus (≈10%) and a rather small jump of the specific heat that translates into a change in entropy at melting $\Delta S_{\mathrm{m}} = 6.9$ J mol^{-1} K^{-1}.

Models aiming to account for the temperature variation of $C_{\mathrm{v}}(T)$ for a liquid usually incorporate contributions from ‘kinetic’ and ‘structural’ sources that include both long-range

mass diffusion and those related to the liquid structure. More specifically, statistical-physics models to calculate the constant-volume specific heat $C_v(T)$ have been proposed for many decades [11]. Expressions such as the following:

$$C_v(T) = 3R/2 + 2\pi\rho^2 \int_0^\infty \left[\left(\frac{\partial g(r)}{\partial T} \right)_V \Phi(r) + \left(\frac{\partial \Phi(r)}{\partial T} \right)_V g(r) \right] r^2 \, dr \qquad (3)$$

where $\Phi(r)$ stands for the effective potential and $g(r)$ for the probability of finding a second particle at a distance r from the reference particle, give a semiquantitative estimate of the temperature dependence of the specific heat. However, an evaluation of the predictive capabilities of equation (3) requires detailed experimental information on $(\partial g(r)/\partial T)_V$ and on the corresponding derivatives for the potential term that are usually hard to obtain.

A route to gain information on the relative importance of 'kinetic' and 'structural' sources on $C_v(T)$ is given by the measurement of some dynamic properties that are sensitive to both kinds of motions. For a simple liquid these involve translational mass diffusion that, within the normal-liquid range, occurs with rates of the order of 10^{-9} m^2 s^{-1} as well as correlated particle motions. The latter in turn comprise both wave and stochastic particle motions, observable at hydrodynamic scales as dilatational and shear waves or as high-frequency collective modes with characteristic scales of 10^{12} Hz [12] as well as motions having an average zero frequency that involve collective rearrangements of neighbours of a 'tagged particle' that take place as a consequence of its diffusion steps.

Our aim here is to illustrate our present level of understanding of the dynamics of simple liquids by means of a case study of a molten alkali metal, as well as how such results could help our understanding of the basic thermodynamic phenomena of the liquid state. These kinds of studies have experienced a renewed interest as the commissioning of new experimental tools, such as inelastic x-ray scattering [13] or nuclear resonance methods using synchrotron radiation [14], brought forward new capabilities, allowing the exploration of uncharted parts of the momentum-transfer Q–energy-transfer $\hbar\omega$ plane.

2. Experimental details

Here we study liquid K at a temperature close to its melting point ($T_1 = 343$ K $\approx T_m + 7$ K) as well as somewhat above ($T_2 = 453$ K $\approx T_m + 117$ K). A preliminary report concerning data close to melting was given previously [15] and here we will focus on the study of the effect of increasing the temperature as well as on the thermodynamic relevance of the present findings.

The sample was chosen for a number of reasons. First, naturally abundant K is a mostly coherent scatterer of neutrons (the ratio of total cross sections becomes $\sigma_c/\sigma_i = 6.26$). This enables us access to the $S_c(Q, \omega)$ coherent dynamic structure factor that comprises the relevant information about the collective dynamics from the measured cross section and also allows a separate study of $S_i^{q.el}(Q, \omega)$, the incoherent-scattering contribution to the spectra which is the dominant feature at low momentum transfers (Q's) and provides information concerning single-particle motions. Second, molten liquid alkali metals are paradigms of the 'simple-liquid' behaviour, i.e. their thermodynamic properties denote an underlying 'harmonic behaviour' as revealed by the values of the ratio of specific heats $\gamma = C_p/C_v \approx 1$, $C_v/Nk_B \approx 3$R and the spectrum of collective excitations at low Q shows peaks at frequencies $\omega_p = \sqrt{Q^2 k_B T/MS(Q)}$. Finally, previous neutron data that were measured over a restricted portion of the Q, ω plane [16] portray the dynamics close to melting ($T_m = 336.7$ K) as markedly different from other alkali metals. Diffusive motions were found to exhibit a solid-like behaviour reminiscent of those of associated liquids [16], with a large residence time for a particle within a 'cage'.

Two sets of measurements were carried out at the ISIS pulsed neutron source (UK) on a sample contained within a custom-built furnace. The IRIS backscattering spectrometer with PG002 settings for the analyser crystals provided a resolution in energy transfers $\Delta E \approx 2.4$ GHz. The MARI chopper spectrometer was employed using incident energies $E_i = 3.6$ THz ($\Delta E \approx 0.1$ THz), 7.2 THz ($\Delta E \approx 0.24$ THz) and 12 THz ($\Delta E \approx 0.3$ THz). The measurements on IRIS were needed in order to study in detail the translational dynamics that is needed in order to provide a proper modelling of $S^{q.el}(Q, \omega)$, i.e. the quasielastic part of the spectrum including both coherent and incoherent components. These high-resolution measurements were also complemented with those performed at MARI using the lowest E_i that enable the exploration of a wider energy window at the expense of a loss in resolution for energy transfers.

The measurements carried out at MARI were aimed at the precise determination of the coherent-inelastic part of the spectrum $S_c^{inel}(Q, \omega)$.

The experimentally accessible quantity here is the double differential scattering cross sections:

$$\frac{d^2\sigma}{d\Omega\, d\omega} = \frac{1}{4\pi}\frac{k}{k_0}[\sigma_c S_c(Q, \omega) + \sigma_i S_i(Q, \omega)] + \text{higher-order terms} \tag{4}$$

where k/k_0 are the wavenumbers of the out- and incoming neutrons (flux factor to convert neutron density into neutron flux) and $S_i(Q, \omega)$ and $S_c(Q, \omega)$ refer to the incoherent- and coherent-scattering components weighted by their relative cross sections. The measured cross sections are brought to an absolute scale by normalization with the scattering of vanadium foil rolled within the sample volume. A number of corrections need to be applied, such as sample self-attenuation, multiple-scattering and multiexcitation effects. These corrections are carried out following [17]. Once these have been applied we obtain the total intensity $I(Q, \omega)$ that fulfils

$$\begin{aligned} I(Q, \omega) &= A[S(Q, \omega) \otimes R(Q, \omega)] \\ S(Q, \omega) &= \frac{\sigma_i}{\sigma_i + \sigma_c} S_i(Q, \omega) + \frac{\sigma_c}{\sigma_i + \sigma_c} S_c(Q, \omega). \end{aligned} \tag{5}$$

Here A is a global scaling constant and $R(Q, \omega)$ is the appropriate instrument resolution function that depends on the instrument and on its specific configuration and is determined by the scattering of thin vanadium foil.

3. Data analysis and results

3.1. Quasielastic spectra

Let us first consider the spectra $I^{q.el}(Q, \omega) \propto S^{q.el}(Q, \omega)$, i.e. the quasielastic part centred at zero frequencies. It can be isolated from the total spectrum in high-resolution measurements performed under conditions where the incident energy is too low to populate the high-frequency collective modes (i.e. $E_i < 2.6$ THz). For our sample it contains both coherent and incoherent components that can only be isolated in polarization analysis experiments. However, at low wavevectors quasielastic scattering is dominated by its incoherent part $S_i^{q.el}(Q, \omega)$ since the coherent counterpart $S_c^{q.el}(Q, \omega)$ shows an intensity which is modulated by the static structure factor $S(Q)$ shown in figure 3. Two representative spectra measured for the two temperatures at midrange of the explored wavevectors are shown in figure 4.

Thermodynamic and transport data pertaining to the two temperatures under consideration are available in the literature [18]. Relevant values for the macroscopic self-diffusion

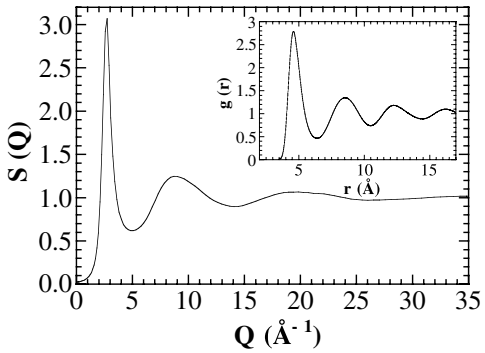

Figure 3. Static structure factor for liquid K close to freezing. Data are taken from [19]. The inset shows a $g(r)$ radial distribution as computed from molecular dynamics.

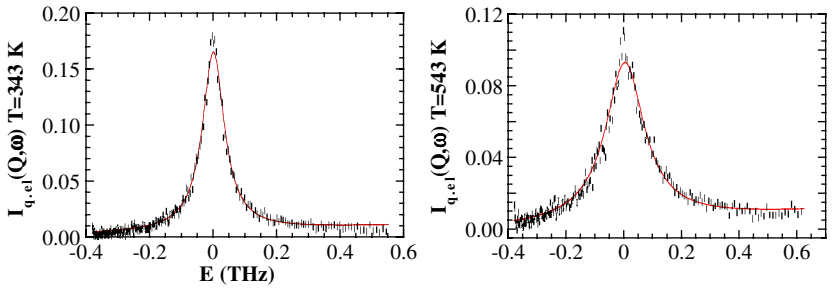

Figure 4. A sample of quasielastic spectra measured on IRIS for a wavevector $Q = 0.7$ Å^{-1}. The full line going through the experimental points is a fit to the model that includes incoherent and coherent contributions as described in the text.

coefficient are 0.38 and 0.67 Å^2 ps^{-1}, those for the shear viscosity are 0.521 and 0.327 mPa s and finally number densities of 0.012 76 and 0.012 36 atoms Å^{-3} are found.

At low wavevectors one expects $S_{\rm i}^{\rm q.el}(Q,\omega)$ to follow a prescription based upon kinetic theory [12, 20] that has been previously tested on molten Na, which is a mostly incoherent scatterer of neutrons [21]. It predicts a quasielastic spectrum with linewidth $\Delta\omega(Q)$ and amplitude $S_{\rm i}^{\rm q.el}(Q,0)$ that deviates from the long-range Fickian diffusion law following

$$\Delta\omega(Q) = DQ^2 - H(\delta)Q/Q^* \tag{6}$$

$$S_{\rm i}^{\rm q.el}(Q,0) = [1 + G(\delta^{-1})Q/Q^*]/\pi DQ^2. \tag{7}$$

Here D stands for the self-diffusion coefficient, $Q^* = 16\pi MnD^2\beta$, M is the particle mass, n is the number density, $\delta = D/(D + \eta/Mn)$ with η being the shear viscosity [9] and $\beta = 1/k_{\rm B}T$. The functions $G(\delta^{-1})$ and $H(\delta)$ are given by Moontfrooij *et al* [12] in a parametric form. The first terms in equation (6) stand for hydrodynamic diffusion and the second terms account for the coupling of mass diffusion with the collective modes. Figure 5 shows how the predictions of equations (6) fare with respect to the measurement. Such an agreement validates the use of the mode-coupling formulae to represent $S_{\rm i}^{\rm q.el}(Q,\omega)$ that does not involve any free parameter. The departure of $\Delta\omega(Q)$ from hydrodynamics can be made more precise if we take as a reference state that described by a regime of binary collisions as

depicted by the Enskog theory. It predicts a diffusion coefficient D_E [2]

$$D_E = \frac{1}{16}\sqrt{\frac{\pi k_B T}{M}}\left(\frac{6}{\pi n y^2}\right)^{1/3}\frac{(1-y)^3}{1-y/2} \tag{8}$$

that is given in terms of the packing fraction $y = \pi n d^3/6$ and the hard-sphere diameter d. The ratios D/D_E give an indication of such a deviation and here we found that such quantities are for both temperatures 0.68 and 0.95, respectively. The strong reduction of the diffusion coefficient with respect to the Enskog value close to melting and its near equality at the higher temperature can be explained on more quantitative grounds following [21] by writing

$$\frac{1}{D} = \frac{\tilde{M}_v^B + \tilde{M}_v^{MC}}{k_B T/M} \tag{9}$$

where $\tilde{M}_v^B$ and $\tilde{M}_v^{MC}$ stand for binary and mode-coupling contributions to the Laplace transform of the memory function for the velocity autocorrelation taken at $z = 0$. From here we can evaluate the strength of the mode-coupling contribution that yields [21]

$$\tilde{M}_v^{MC} = \frac{k_B T/M}{D}\left[1 - \frac{D}{D_E}\right]. \tag{10}$$

Our data using a value of $d = 4.09$ Å yield values for $\tilde{M}_v^{MC}$ of 5.93 and 0.69 for the two temperatures, respectively. The large and positive value for the temperature close to melting reflects the presence of a strong coupling between diffusion and density fluctuations, while at somewhat higher temperatures such coupling is far weaker. In fact, for $T \approx 485$ K such a term changes sign and for higher temperatures the result is now an enhancement of the diffusion with respect to the Enskog value.

As regards $S_c^{q.el}(Q, \omega)$ there seems to be no widely accepted model to account for the shape and width of this spectral component, an exception being the region about Q_p, i.e. where $S(Q)$ shows its maximum. The experimental data for this component was analysed using a Lorentzian with adjustable width and an amplitude bound to the relative cross section. The Q dependence of such a linewidth, also plotted in figure 5, shows a minimum at Q_p, where $S(Q)$ shows its main maximum and can be accounted for semiquantitatively by [22]

$$\Delta\omega_c(Q) = \frac{\Delta\omega(Q)}{S(Q)[1 - j_0(QR_0) + 2j_2(QR_0)]}. \tag{11}$$

Here R_0 corresponds to an atomic diameter and its value is set to that corresponding to the main minimum in the $V(r)$ pair interaction potential [4], $j_x()$ stand for spherical Bessel functions and use is made of the $\Delta\omega(Q)$ instead of Fickian diffusion. As seen there the agreement between theory and experiment for wavevectors below Q_p is only qualitative.

Our present understanding of the stochastic dynamics thus portrays quasielastic scattering as arising from diffusive motions that enable a density fluctuation to relax. Close to T_m the diffusion is hampered with respect to the Enskog case since the particle oscillates for a given time within a 'cage' constituted by surrounding particles which hinder its forward motion. At liquid densities close to melting, the most significant modes that couple to translational diffusion seem to be those with wavevectors close to Q_p [21]. Long-range diffusion thus sets in when a longitudinal collective mode with wavevector Q_p carries the tagged particle together with its nearest neighbours between different spatial positions. Such a coupling thus gives rise to motions of a group of particles that results in a coherent quasielastic spectrum showing a modulation of $\Delta\omega_c(Q)$ versus Q while its amplitude follows the oscillations of $S(Q)$.

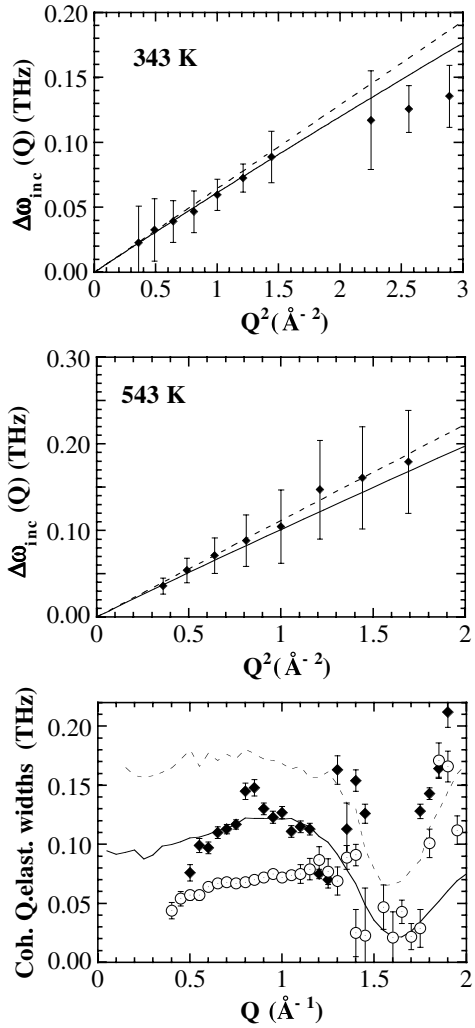

Figure 5. The two upper frames compare the experimental quasielastic incoherent linewidth (lozenges) with hydrodynamic diffusion (full lines) as well as the mode-coupling prediction given by equations (6). The lowest frame compares the experimental estimates for the quasielastic linewidths (open circles 343 K, lozenges 453 K) with the predictions made from equation (11).

3.2. Spectra for the collective modes

At low Q the spectrum of collective density fluctuations shows the Rayleigh–Brillouin triplet as predicted by linearized hydrodynamics [5]. As Q increases and crosses the hydrodynamic limit (usually within the range of $Q \approx 10^{-2}$ Å^{-1}) the width of the Brillouin lines increases due to the onset of scattering processes that limit the lifetime of the underlying excitations. For potassium at melting, estimates for the lifetime of a longitudinal phonon at the zone boundary [23] yields a value of 0.56×10^{-12} s, a figure that sets an upper limit for the lifetimes of the excitations persisting in the molten state. The mean-free path for such a phonon within the hot crystal reduces to $\approx$11 Å, a quantity smaller than the static correlation length within the liquid above melting, as can be judged from the spatial extent of the oscillations in the partial

pair static correlation function shown in figure 3. We thus expect to observe in the liquid state excitations that can be considered as remnants of those present in the hot crystal since the local structures of the crystal and liquid at such scales of length are not too different.

Models to analyse the $S^{\mathrm{inel}}(Q,\omega)$ spectra of collective excitations are often built on plausibility grounds [12] using a model to represent the inelastic wings supplemented by a 'fitting function' for the quasielastic region. Here, we seek an alternative representation for $S_{\mathrm{c}}^{\mathrm{inel}}(Q,\omega)$ that extends the usual 'three-pole approximation' [5] that gives the spectral lineshape in terms of the first two even reduced frequency moments of $S_{\mathrm{c}}(Q,\omega)$:

$$\omega_0^2 = \frac{1}{S(Q)}\int \mathrm{d}\omega\,\omega^2 R(Q,\omega) = \frac{Q^2 k_{\mathrm{B}}T}{MS(Q)} \tag{12}$$

$$\omega_{\mathrm{l}}^2 = \frac{1}{\omega_0^2 S(Q)}\int \mathrm{d}\omega\,\omega^4 R(Q,\omega) \tag{13}$$

and a relaxation time $\tau = [(\omega_{\mathrm{l}}^2 - \omega_0^2)/\pi]^{-1/2}$. Here, $R(Q,\omega) = S_{\mathrm{c}}(Q,\omega)(1 - \exp(-\hbar\omega/k_{\mathrm{B}}T)/\omega)$ and a closed form expression for the spectral shape is

$$R(Q,\omega) = \frac{1}{\pi S(Q)}\frac{\omega_0^2(\omega_{\mathrm{l}}^2 - \omega_0^2)\tau}{[\omega\tau(\omega^2 - \omega_{\mathrm{l}}^2) + (\omega^2 - \omega_0^2)^2}. \tag{14}$$

The second moment is easily calculated using experimental data for $S(Q)$ from [19], while the fourth and the sixth depend upon details of the interaction potential. For ω_{l} an approximate formula is given in terms of R_0 and a parameter, ω_{E}, playing the role of an Einstein frequency [5] and gives

$$\omega_{\mathrm{l}}^2 \doteq \frac{3Q^2 k_{\mathrm{B}}T}{M} + \omega_{\mathrm{E}}\left[1 - \frac{3\sin(QR_0)}{QR_0} - \frac{6\cos(QR_0)}{(QR_0)^2}\frac{6\sin(QR_0)}{(QR_0)^3}\right]. \tag{15}$$

Equation (14) predicts the appearance of well defined inelastic sidepeaks when the condition $3\omega_0^2 > \omega_{\mathrm{l}}$ holds as well as a linewidth for the coherent part of the quasielastic spectrum that varies linearly with the wavevector. While equation (14) yields a good account of spectra measured at the higher temperature using as parameters $R_0 = 4.7$ Å and $\omega_{\mathrm{E}} = 1.69$ THz, the analysis of data close to melting was found to require a somewhat more elaborate treatment since no reasonable value for the referred parameters could be found. For such a purpose we sought to refine the expression for the dynamic structure factor that is written in terms of the memory function $\tilde{M}(Q,\mathrm{i}\omega)$:

$$S_{\mathrm{c}}(Q,\omega) = \frac{\omega\beta S(Q)}{1 - \mathrm{e}^{(-\hbar\omega\beta)}}\,\mathrm{Re}[\mathrm{i}\omega + \tilde{M}(Q,\mathrm{i}\omega)]^{-1}, \tag{16}$$

where the tilde stands for Laplace-transformed quantities.

The memory function is often specified by a continued fraction:

$$\tilde{M}(Q,s) = \omega_0^2[s + \tilde{K}^{(1)}(Q,s)]^{-1} \tag{17}$$

with $\tilde{K}^{(n)}(Q,s) = K^{(n)}(Q,t=0)[s + \tilde{K}^{(n+1)}(Q,s)]^{-1}$. The usual approach terminates the continued fraction at $n = 1$ based upon the assumption that $K^{(2)}(Q,t)$ decays too fast within our time window, i.e. $\tilde{K}^{(2)} = 1/\tau$. This can be improved by going one step further. In doing so one arrives at

$$\tilde{M}(Q,s) = \omega_0^2\left[s + \frac{\omega_{\mathrm{l}}^2 - \omega_0^2}{s + (\omega_{\mathrm{s}}^4 - \omega_{\mathrm{l}}^4)/(\omega_{\mathrm{l}}^2 - \omega_0^2)(s + 1/\tau)}\right]^{-1}, \tag{18}$$

where ω_{s}^4 is the ratio between the sixth normalized moment and ω_0^2.

Figure 6 shows representative spectra measured at MARI as well as the approximation given in terms of equation (16) using as adjustable parameters τ, ω_{s} and ω_{l} as well as the

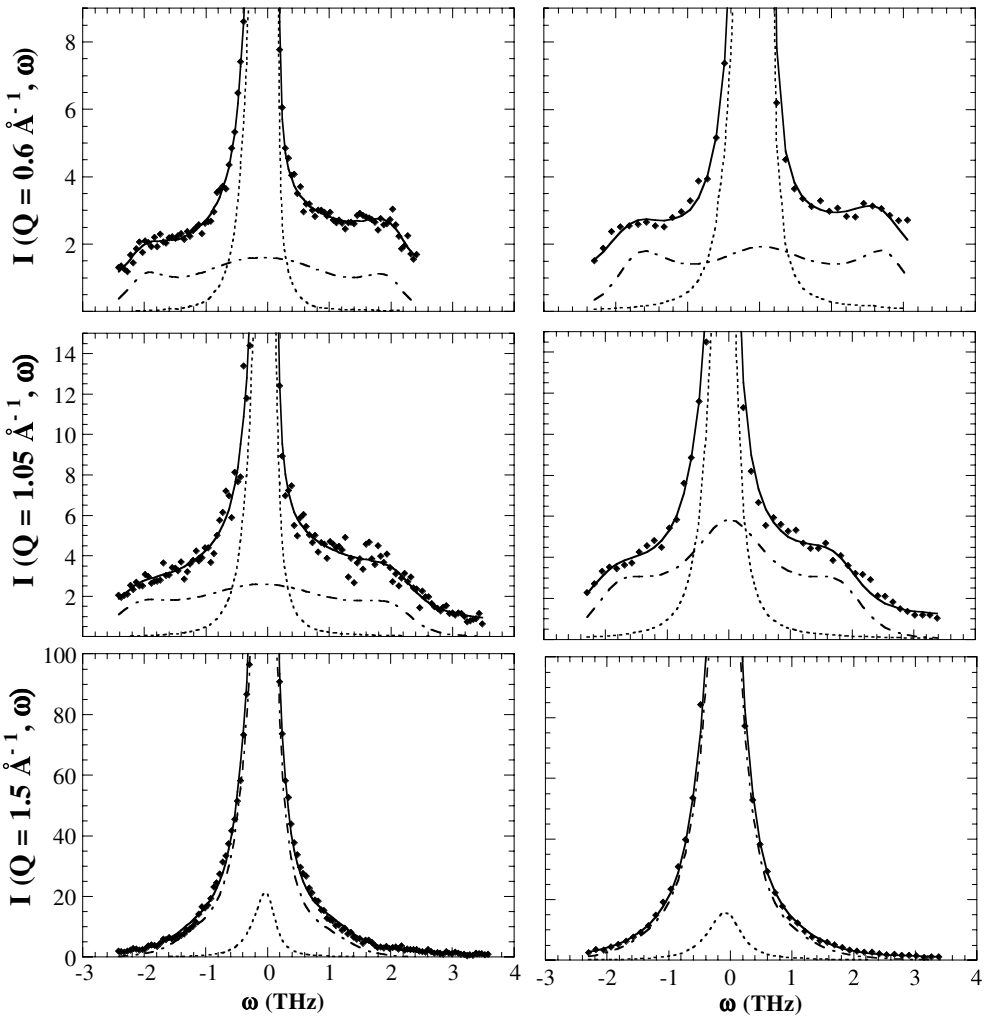

Figure 6. A set of spectra measured on MARI for three representative wavevectors. The left-hand column depicts spectra for $T = 343$ K and that on the right-hand side those for $T = 453$ K. Experimental data points are depicted by full symbols. Thick full curves show the fitted model using equation (16). The broken curve shows the symmetrized inelastic intensity as predicted by equation (16) and the dotted curve depicts the quasielastic contribution.

scale factor A. Inelastic side peaks are seen in the spectra for $Q \leqslant 1.3$ Å for $T = 343$ K which are indicative of the presence of propagating density oscillations and become somewhat more blurred at $T = 453$ K.

Figure 7 displays plots for ω_0 and ω_l calculated as described in [5] as well as the estimate for the latter if left as a free parameter. For most wavevectors the calculated and fitted values for this quantity are very close, which validates the use of the extended model given by equations (16)–(18). The hydrodynamic linear dispersion $c_T Q$ given by the macroscopic isothermal sound velocity $c_T = 1605$ m s^{-1} for $T = 343$ K and $c_T = 1529$ m s^{-1} for $T = 543$ K approaches ω_0 from above for $T = 543$ K approaches ω_0 from above for $Q \leqslant 0.3$ Å^{-1} and $Q \leqslant 0.45$ Å^{-1} for both temperatures, respectively. However, both frequencies ω_m corresponding to the maxima

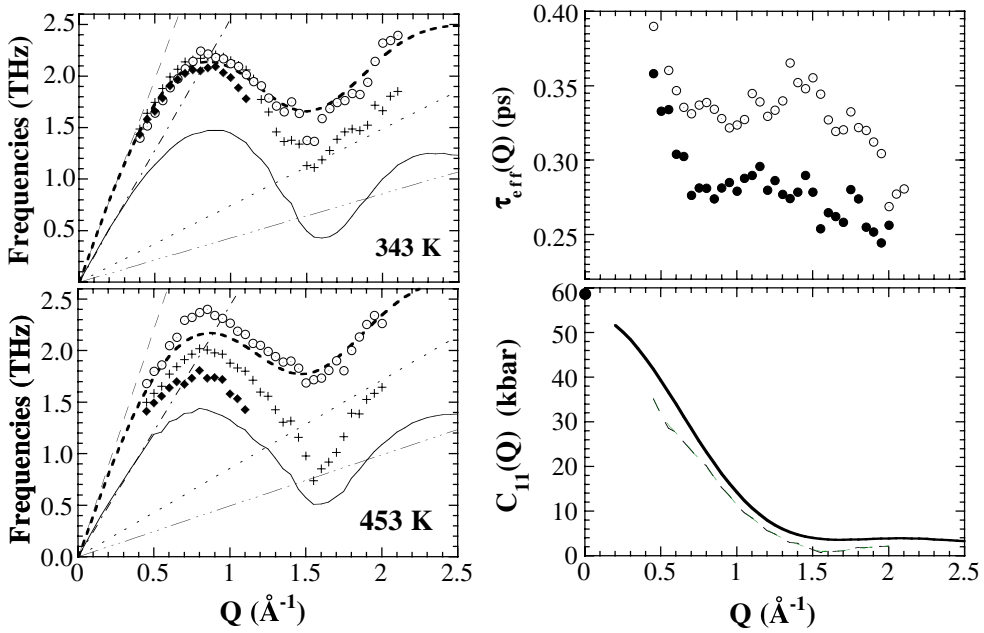

Figure 7. The left-hand frames show the excitation frequencies for both temperatures. Estimates for the square root of the reduced second frequency moment ω_0 are given by the full curves. The chain curves represent hydrodynamic dispersion $\Omega_{\rm hyd} = c_{\rm T} Q$ and the long broken curves stand for $c_\infty Q$ (see the text). The square roots of the reduced fourth frequency moments are shown by circles with a dot when $\omega_{\rm l}$ is left as a free parameter and the short broken curves show the estimates for this quantity if calculated using equation (15) with parameter values $\omega_{\rm E} = 1.55$ THz and $R_0 = 4.62$ for 343 K and $\omega_{\rm E} = 1.69$ THz and $R_0 = 4.70$ for $T = 453$ K. The full symbols give the $\omega_{\rm m}$ peak frequencies and the crosses show the $\omega_{\rm ml}$ maxima of the longitudinal current $J_{\rm L}(Q, \omega)$ correlations as calculated from the fitted spectra. The upper-right frame depicts the effective lifetimes $\tau_{\rm eff}$ as derived from the model fits for 343 K (open symbols) and 453 K (full dots). The lower-right frame shows the wavevector dependence of the $C_{11}(Q)$ elastic moduli. The full line shows data for K as derived from $\omega_{\rm l}$. The thick full symbol at $Q = 0$ shows the value calculated from bulk and rigidity moduli of the room temperature crystal.

of the inelastic side peaks and those $\omega_{\rm ml}$ derived from the maxima of the longitudinal current $C_{\rm L}(Q, \omega) = \omega^2 S(Q, \omega)/Q^2$ calculated from the fitted spectra are significantly above ω_0. Since $\omega_{\rm ml}$ are equivalent to the characteristic frequencies of a damped harmonic oscillator they may be considered as the true physical frequencies of the oscillatory motion under scrutiny.

At $T = 343$ K damping effects become increasingly important for $Q > 0.6$ Å^{-1}. This is easily seen by the difference between $\omega_{\rm ml}$ and $\omega_{\rm m}$. Moreover, for $Q > 1.3$ the excitations enter an overdamped regime. The damping effects are far more noticeable at $T = 453$ K, as is also shown by the larger differences between such frequencies. To quantify the lifetime of the excitations at both temperatures, a relaxation time is defined in terms of the ratios of the higher-frequency moments $\tau_{\rm eff} = \tau(\omega_s^4 - \omega_{\rm l}^4)/(\omega_{\rm l}^2 - \omega_0^2)^2$. This amounts to considering $\tilde{K}^{(3)} = 1/\tau$ that corresponds to the additional level employed in the continued-fraction expression given by equation (18). The assignment to such a parameter with an excitation lifetime relies on its strict equivalence to such a quantity (i.e. the width of the Brillouin peaks) that occurs as one approaches the hydrodynamic regime. The result is shown in the upper-left frame of figure 7 and shows that the lifetimes at temperatures close to melting are at most 0.35 ps, leading to mean-free-paths of about 6 Å. Increasing the temperature has a deleterious effect on the lifetimes that

now get substantially reduced. Data for $\omega_{\rm m}$, $\omega_{\rm ml}$ and $\omega_{\rm l}$ approach the $Q \to 0$ hydrodynamic realm in a way not too different from that followed by other alkali metals [12] showing a large amount of positive anomalous dispersion. The linear dispersion approached by such data is given by the high-frequency sound velocity $c_\infty = \sqrt{(3/\beta M) + (3\omega_{\rm E}^2 R_0^2/10)} = 2490$ m s^{-1} for 343 K and 2778 m s^{-1} K of an elastic medium being sampled 'instantaneously' by a high-frequency probe.

The mechanisms leading to such large velocity dispersions are understood from classical hydrodynamics. At frequencies well above $\mathcal{B}_{\rm T}/\eta \approx 1$ THz, where $\mathcal{B}_{\rm T}$ stands for the isothermal bulk modulus, the linearized form of the Navier–Stokes formulae become invalid [24]. The propagation of a density oscillation is then governed by the equations of motion for an isotropic solid that lead to a dispersion $\omega^2/Q^2 = (\mathcal{B} + \frac{4}{3}\mathcal{G})/Mn$. A connection with quantities just considered is made in terms of the wavevector- dependent modulus [5]

$$C_{11}(Q) = \frac{Mn\omega_{\rm l}^2}{Q^2}, \qquad \lim_{Q\to 0} C_{11}(Q) = \mathcal{B} + \tfrac{4}{3}\mathcal{G}. \tag{19}$$

Information on $C_{11}(Q)$ obtained from $\omega_{\rm l}$ is given in figure 7 that also displays the macroscopic ($Q \to 0$) value calculated for solid K at room temperature [25]. There we see that the liquid data comes close to the value for the crystal at long wavelengths. The agreement between the liquid and crystal data, which is also exemplified by the macroscopic data for the bulk moduli shown in figure 2, is understood from the small variations experienced by the density upon melting that makes the short-range structure of the liquid, and thus the forces driving the atomic dynamics, to show a relatively mild change after the crystal structure is lost.

4. Discussion

4.1. Vibratory motions versus diffusion

The picture drawn above portrays high-frequency vibratory motions as a remnant of those from their parent crystals at temperatures close to melting. Such motions correspond to relatively short-lived configurations that become unstable after a fraction of a picosecond. Particle dynamics at longer times is dominated by collisions with its neighbours that follow a given particle on its long-range diffusion track. To compare the extent of vibratory and diffusive motions on more quantitative grounds we show in figure 8 the results of an analysis carried out following the instantaneous normal mode scheme [26] of some recent molecular dynamics results. The basics of the method consists in taking from the simulation an instantaneous N-particle configuration, expanding the potential energy about such a configuration and from there calculating the force-constant and first-derivative matrices. The procedure is averaged over a significant number of configurations and, after completion, diagonalization of the $3N$-dimensional force-constant matrix yields a set of individual particle eigenvalues and eigenvectors. The obtained frequencies, that may be real or imaginary depending upon the stability of a given mode, are usually plotted as a density of states $Z_{\rm INM}(\omega)$ on a frequency axis including negative (unstable) and positive (stable) lobes, as is shown in figure 8. The positive lobe of $Z_{\rm INM}(\omega)$ is thus an analogue to the phonon density of states of the crystal, and indeed it is an easy matter to see that the extent in frequencies of both crystal and $Z_{\rm INM}(\omega)$ are comparable, with the exception of the lowest- and highest-frequency sides which show in the liquid an excess of states with respect to the crystal. From figure 8 we see that increasing the temperature from close to melting to $T/T_{\rm m} = 1.33$ leads to a decrease in the number of stable modes for frequencies of 0.9–2.9 THz and an increase in the number of unstable modes with frequencies -0.25 to -1.4 THz and a small shift of the centre of gravity $\langle\omega^{\rm u}\rangle$ of the

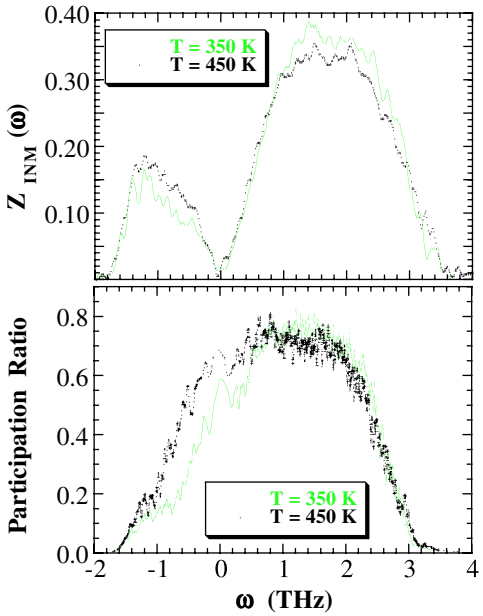

Figure 8. The upper frame shows the spectral distribution of instantaneous normal modes. The lower frame depicts the participation ratio.

distribution for unstable modes from −1.21 to −1.22 THz. The fraction of unstable modes f_u (i.e. the relative area of the lobe of unstable frequencies) increases from 0.16 at 343 K to 0. 20 at $T = 453$ K, which results in a concomitant decrease of the fraction of stable harmonic modes from 0.84 to 0.80. Since the diffusion coefficient is known to follow $D \simeq (\langle\omega^u\rangle f_u)^\gamma$ with $\gamma \approx 1$ we see that the increase in temperature results in a strong increase of the diffusion coefficient and a concomitant decrease in the density of finite-frequency harmonic modes.

As regards the number of atoms participating in a given mode, figure 8 also shows the participation ratio defined through the mode eigenvectors [26]. The main result here concerns the strong increase with temperature in the number of atoms that take part in unstable and low-frequency stable modes which occur up to frequencies of ≈1 THz. The increase in the value of the self-diffusion coefficient is thus accompanied by an increase in the number of atoms that execute such motions. In contrast, the percentage of atoms taking part in vibrational motions does not experience a very significant variation.

4.2. Dynamics versus thermodynamics

From results described in the previous section we expect the contribution of finite-frequency vibrations to the specific heat to decrease with increasing temperature because of the decrease in the density of modes referred to above. As regards that corresponding to diffusive motions we expect that it will increase with temperature, as expected from simple kinetic considerations as well as from the increase in the participation ratio referred to above. A direct quantitative estimate of how these findings lead to the observed variation of $C(T)$ seems, however, out of reach. Alternatively, a connection between what is observed experimentally and the T dependence of the specific heat can be sought on the grounds of semi-phenomelogical approaches. To pursue such a route we follow the steps of [7] that decompose the specific

heat into an ion-motion and an electronic part $C_v = C_I + C_E$. The latter, which amounts to 0.080 in units of R, can be easily estimated for free-electron liquids by means of band-theory calculations that yield $C_E = \pi^2 N k_B T n(\epsilon_F)$ [8] in terms of $n(\epsilon_F)$, i.e. the electron density of states per atom at the Fermi energy. The difference $C_v - C_E$ yields a ion-motional contribution [7, 8]

$$C_I = 3R + C_{anh} + C_b \tag{20}$$

where the first term is the quasiharmonic contribution and is the major part of C_I, while C_{anh} is the anharmonic contribution which is found to be a universal function of the reduced temperature T/T_m with values ranging from $0.4R$ at T_m to zero for $T \geqslant 2T_m$. Both contributions show values not too different from those of the hot crystal for which they are the only contributions to the specific heat. For the liquid the additional C_b 'boundary' term [7] accounts for the existence within the liquid of potential valleys which do not extend infinitely in all directions but are truncated along some directions that coincide with intersections between potential energy valleys. Such a term is negative and varies from zero at T_m to $-0.6R$ at $T = T_m$. It is thus such a term that makes C_v decrease in value from that at melting at higher temperatures.

Models to evaluate C_b have appeared [7] and its explicit evaluation requires information about the frequencies ω_λ and amplitudes a_λ of the N ions composing the liquid or some average quantities pertaining to both. The expression is [7]

$$\begin{aligned} C_b &= -k_B \sum_\lambda B_\lambda (b_\lambda^2 + \tfrac{1}{2} + B_\lambda) \\ B_\lambda &= \frac{b_\lambda \exp(-b_\lambda)^2}{\sqrt{\pi}\,\mathrm{erf}\, b_\lambda} \\ b_\lambda &= \sqrt{M\omega_\lambda^2 a_\lambda^2 / 2k_B T}. \end{aligned} \tag{21}$$

The frequencies ω_λ comprise both diffusive and oscillatory motions studied in the experiment just described and extend from zero up to a high-frequency cut-off. An approximate separation of both kinds of motion is accomplished with the help of frequency spectra $Z(\omega)$ such as that shown in figure 9 calculated from computer molecular dynamics. The curves shown there have an ordinate at the origin proportional to $2MD/\pi k_B T$ and can be decomposed into two bands representing diffusive and oscillatory regions with the aid of models for $Z(\omega)$ given in [27]. There [27], the total $Z(\omega)$ is decomposed into an oscillatory part characterized by a single frequency ω_{osc}, a friction constant μ_{osc} and a parameter a_{osc} related to the inverse of the oscillation lifetime and a stochastic part specified by the self-diffusion coefficient and an additional friction term γ_r that only affects the stochastic forces. The expression just referred to is [27]

$$Z(\omega) = \frac{2MD}{\pi k_B T}\left[\frac{f^2}{(\omega^2 + \mu_{osc}^2)\omega_{osc}^2 + f^2} + \frac{f}{\omega_{osc}^2}\frac{\omega^2 a_{osc}}{\mu_{osc}^2}\right]\left[\left(\frac{\omega^2 - \omega_{osc}^2}{\omega_{osc}^2}\right)^2 + \frac{\omega^2 a_{osc}^2}{\omega^2 + \mu_{osc}^2}\right]^{-1} \tag{22}$$

with $f = \gamma_r \mu_{osc}$, the self-diffusion coefficients set to the macroscopic values and the rest of the parameters left as adjustable. Parametric fits to the equation given above and the corresponding results shown in figure 9 tell us that the approximation has to be regarded as of semi-quantitative nature. The best-fit values for the oscillation frequencies $\omega_{osc} = 1.80$ and 1.76 THz for the two temperatures are not too far from the estimates for the Einstein frequencies quoted above, the friction terms μ_{osc} identifiable with viscous effects decrease by 41% to be compared with a drop of 37% in the shear viscosity and finally the parameter a_{osc} that varies from 1.207 at 343 K to 1.223 at 453 K, which is interpreted as a decrease in oscillation lifetime of a mere 2%. Also, the parameter γ_r associated with diffusive motions drops 1.6 times with increasing

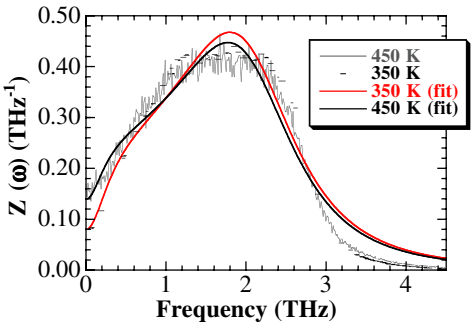

Figure 9. Normalized spectral frequency distributions as calculated from the velocity autocorrelation functions corresponding to a molecular dynamics simulation on molten K at 350 and 450 K. Both distributions are normalized to unit area. The full and dotted curves are approximations to both frequency spectra calculated using equation (22).

temperature, which compares with the ratio of 1.4 times expected on the grounds of Brownian dynamics (i.e. $\gamma_r \approx k_B T/MD$). With such provisos in mind we use the expression given above to carry out an approximate separation of the frequency spectrum into a diffusive and an oscillatory part. As for the mode amplitudes, the following simplifying assumptions were undertaken:

(a) the motions comprising mass diffusion were assigned a common amplitude given by the Langevin formula so that $a_\lambda^2 = 6MD^2/k_B T$,
(b) those corresponding to the vibrational displacements were approximated by $a_\lambda = c(Q)\tau_{\text{eff}}$, where $c(Q) = \omega_Q/Q$ is the phase velocity of the collective excitation and τ their lifetimes as estimated from measurement.

Finally the frequency interval where $Z(\omega)$ shows non-zero values (up to ≈5 THz) was divided into bins of widths comparable with the achieved instrument resolution (≈0.3 THz). Under such simplifying assumptions one gets $C_b = -0.02R$ and $-0.06R$ for the two temperatures under consideration. The values for the total constant-volume specific heat are then compared with experimental data in figure 2 and found to be in fair agreement. The magnitude of C_b at temperatures not far from melting is thus comparable to that of electronic origin ($0.08R$) but significantly smaller than that accounting for anharmonic effects ($0.4R$).

5. Concluding remarks

Studies on the dynamics of simple liquids, such as the light molten alkali metals (Li, Na) [12], have experienced a greater interest recently due to the new experimental capabilities brought forward by third generation synchrotron sources that allow the measurement of excitations free from the kinematic restriction inherent to neutron scattering [13]. The present data complement the well studied cases of the heavier alkalis (Rb,Cs) explored by means of neutron spectroscopy and those of the lighter Li and Na examined with the x-ray technique [12]. Our interpretation of the origin of the high-frequency sound velocity can easily be extended to the other alkali metals for which elastic-constant data are available (Li, Na and Cs, [25]). The values calculated from elastic data of the hot crystals yield phase velocities of 6692 m s^{-1} (Li), 3545 m s^{-1} (Na) and 1363 m s^{-1} (Cs), which compare with reported values for liquids of ≈6500, 3025 and 1061 m s^{-1}, respectively.

At the present moment, one of the main limitations of the inelastic x-ray technique concerns the achievable energy resolution which can hardly be improved beyond ≈1 meV without reducing the photon flux down to impractical limits. There is, however, a number of significant studies that can be done using both techniques in a complementary fashion such as using neutron scattering to study in detail the quasielastic spectrum of the lighter alkalis using such information for a proper modelling of the $S^{\mathrm{inel}}(Q, \omega)$ measured by x-rays. Such complementarity is even more evident in the case of more complex liquids such as transition metals [28], semimetals [29] or alloys [30]. Here the kinematic range available to neutron scattering is severely limited but, in contrast, information from high-resolution inelastic- and quasielastic neutron scattering will certainly solve some apparent disagreements between results derived from both techniques.

Complex molecular materials have also been examined using the inelastic scattering of x-rays [31]. An assessment of the results obtained must, however, take into account the usually large number of low-lying excitations of different nature from the 'acoustic' phonons that contribute to the measured spectral intensity [32], a fact well known from studies on polycrystals [13], and are dumped together in most analysis of experimental data. In this respect, establishing connections between observation at microscopic scales and thermodynamics provide a safeguard against oversimple interpretations of experimental data. Finally, high sound-velocity materials, such as molten alumina [33] or liquid alloys of geophysical interest to be studied under extreme conditions (i.e. FeNiS or FeNiSi) where the 'acoustic' excitations can be isolated experimentally, are some examples where such techniques are being profitably applied.

Acknowledgment

This work was supported in part by grant no MAT2002-04540-C05-03 (Spain).

References

[1] Herring C 1950 *J. Appl. Phys.* **21** 437
[2] Faber T E 1972 *Theory of Liquid Metals* (Cambridge: Cambridge University Press) ch 3, p 154
[3] Rahman A 1964 *Phys. Rev.* A **136** 405
[4] Lai S K, Wang Li and Tosi M P 1990 *Phys. Rev.* A **42** 7289
[5] Lovesey S W 1986 *Theory of Neutron Scattering from Condensed Matter* (Oxford: Oxford Science Publications) ch 5
Bryk T and Mrygold I 2001 *Phys. Rev.* E **63** 051202-1
[6] Granato A V 2002 *J. Non-cryst. Solids* **307–310** 376
Jones H D 1973 *Phys. Rev.* A **8** 3215
[7] Wallace D C 1998 *Phys. Rev.* E **57** 1717
[8] Wallace D C 1997 *Phys. Rev.* E **56** 4179
[9] IIda T and Guthrie R I L 1993 *The Physical Properties of Liquid Metals* (Oxford: Oxford Science Publications) ch 4, p 90
[10] Brillouin L 1937 *Trans. Faraday Soc.* **33** 54
[11] Croxton C A 1975 *Introduction to Liquid State Physics* (New York: Wiley) ch 3, p 56
[12] Sinn H *et al* 1997 *Phys. Rev. Lett.* **78** 1715
Scopigno T *et al* 2000 *Phys. Rev. Lett.* **85** 4076
Moontfrooij W *et al* 1986 *Phys. Rev.* A **33** 1405
Pilgrim W C *et al* 1999 *J. Non-Cryst. Solids* **250–252** 96
Bove L E *et al* 2000 *Phys. Rev. Lett.* **85** 5352
Copley J R D and Rowe J M 1974 *Phys. Rev. Lett.* **32** 49
Bodensteiner T *et al* 1992 *Phys. Rev.* A **45** 5709
[13] Burkel E 1991 *Inelastic Scattering of X-Rays with Very High-Energy-Resolution* (Berlin: Springer)

[14] Chumakov A I and Ruffer R 1998 *Hyperfine Interact.* **113** 59
Chumakov A I *et al* 1996 *Phys. Rev. Lett.* **76** 4528
[15] Cabrillo C *et al* 2002 *Phys. Rev. Lett.* **89** 075508-1
[16] Novikov A G *et al* 1996 *Physica (Amsterdam)* B **228** 312
Novikov A G *et al* 1997 *Physica (Amsterdam)* B **236–239** 359
Novikov A G *et al* 1996 *J. Phys.: Condens. Matter* **8** 3525
[17] Dawidowski J *et al* 2002 *Nucl. Instrum. Methods* B **195** 389
Dawidowski J, Bermejo F J and Granada J R 1998 *Phys. Rev.* B **58** 706
[18] See IIda T and Guthrie R I L 1993 *The Physical Properties of Liquid Metals* (Oxford: Oxford Science Publications) ch 6, pp 183–5, ch 3, p 71 and ch 7, p 201
[19] van de Lugt W 1985 *Handbook of Thermodynamic and Transport Properties of Alkali-Metals* ed R W Ohse (Oxford: Blackwell) p 102
[20] Wahnström G and Sjögren L 1982 *J. Phys. C: Solid State Phys.* **15** 401
[21] Morkel C and Pilgrim W C 2002 *J. Non-Cryst. Solids* **312–314** 128
[22] Cohen E G D, Westerhuijs P and de Schepper I M 1987 *Phys. Rev. Lett.* **59** 2872
[23] Glyde H R, Hansen J P and Klein M L 1997 *Phys. Rev.* B **16** 3476
Buyers W J L and Cowley R A 1969 *Phys. Rev.* **180** 755
[24] Bhatia A B 1967 *Ultrasonic Absorption* (New York: Dover) p 236
[25] Beg M M and Nielsen M 1976 *Phys. Rev.* B **14** 4266
Woods A D B *et al* 1962 *Phys. Rev.* **128** 1112
Daniels W B 1960 *Phys. Rev.* **119** 1246
Nücker N and Buchenau U 1985 *Phys. Rev.* B **31** 5479
[26] For calculation details as well as some previous results concerning molten Na and Cs see
Wu T M and Tsay S F 1996 *J. Chem. Phys.* **105** 9281
Vallauri R and Bermejo F J 1995 *Phys. Rev.* E **51** 2654 and references therein
[27] Egelstaff P A 1992 *An Introduction to the Liquid State* (Oxford: Oxford Science Publications) ch 12, p 252
The first derivation of the approximation is given by Nakahara Y and Takahashi H 1966 *Proc. Phys. Soc.* **89** 747
[28] Bermejo F J *et al* 2002 *Phys. Rev. Lett.* **85** 106
[29] Bermejo F J, Garcia-Hernandez M, Martinez J L and Hennion B 1994 *Phys. Rev.* E **49** 3358
Bermejo F J *et al* 1997 *Phys. Rev.* E **56** 3358
Scopigno T *et al* 2002 *Phys. Rev. Lett.* **89** 255506
[30] Fernandez-Perea R *et al* 1999 *Phys. Rev.* E **59** 3212
Enciso E *et al* 1998 *Phys. Rev. Lett.* **81** 4432
Alvarez M, Bermejo F J, Verkerk P and Roessli B 1998 *Phys. Rev. Lett.* **80** 2141
Fernandez-Perea R, Alvarez M, Bermejo F J, Verkerk P, Roessli B and Enciso E 1998 *Phys. Rev.* E **58** 4568
[31] See for instance Sette F *et al* 1998 *Science* **280** 1550
[32] Bermejo F J, Cuello G J, Courtens E, Vacher R and Ramos M A 1998 *Phys. Rev. Lett.* **81** 3801
[33] Sinn H *et al* 2003 *Science* **299** 2047